ACS OMEGA

http://pubs.acs.org/journal/acsodf

Article

Synthesis, Characterization, and Utilization of a Lignin-Based Adsorbent for Effective Removal of Azo Dye from Aqueous Solution

Xianzhi Meng,* Brent Scheidemantle, Mi Li, Yun-yan Wang, Xianhui Zhao, Miguel Toro-González, Priyanka Singh, Yunqiao Pu, Charles E. Wyman, Soydan Ozcan, Charles M. Cai, and Arthur J. Ragauskas*

Cite This: *ACS Omega* 2020, 5, 2865−2877

Read Online

ACCESS | Metrics & More | Article Recommendations | Supporting Information

ABSTRACT: How to effectively remove toxic dyes from the industrial wastewater using a green low-cost lignocellulose-based adsorbent, such as lignin, has become a topic of great interest but remains quite challenging. In this study, cosolvent-enhanced lignocellulosic fractionation (CELF) pretreatment and Mannich reaction were combined to generate an aminated CELF lignin which is subsequently applied for removal of methylene blue and direct blue (DB) 1 dye from aqueous solution. ^{31}P NMR was used to track the degree of amination, and an orthogonal design was applied to determine the relationship between the extent of amination and reaction parameters. The physicochemical, morphological, and thermal properties of the aminated CELF lignin were characterized to confirm the successful grafting of diethylenetriamine onto the lignin. The aminated CELF lignin proved to be an effective azo dye-adsorbent, demonstrating considerably enhanced dye decolorization, especially toward DB 1 dye (>90%). It had a maximum adsorption capacity of DB 1 dye of 502.7 mg/g, and the kinetic study suggested the adsorption process conformed to a pseudo-second-order kinetic model. The isotherm results also showed that the modified lignin-based adsorbent exhibited monolayer adsorption. The adsorbent properties were mainly attributed to the incorporated amine functionalities as well as the increased specific surface area of the aminated CELF lignin.

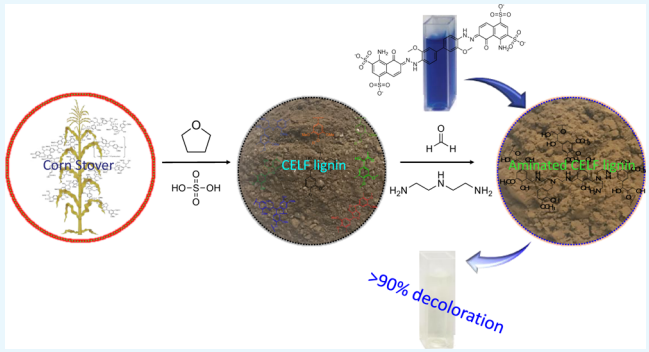

INTRODUCTION

The demand for clean water is likely to increase driven by the rapid urbanization, expanding industrial activities, energy generation, and water pollution. Because of the limited fresh water resources on earth, this demand should be addressed by developing promising water purification techniques. The presence of organic dyes in industrial wastewater could cause some serious environmental concerns because of their poor biodegradability and toxicity to the exposed plants, living organisms, and even human being. As a result, these toxic dyes should be removed from the wastewater as much as possible before being discharged to land or water sources in an environmentally friendly manner.[1] The textile industry consumes organic dyes, which represent 60% of the world's dye consumption, and it was reported that 10−25% of water-soluble dyes is lost during the dyeing process, and 2−20% of dyes is released as the effluent into the water system after the dyeing process.[2] Azo dyes are known as dyes containing −N═N− groups, representing 60−70% of commercially available dyes in the world.[3] They are extensively used in the textile industry and become part of the textile effluents. Therefore, how to cost-effectively remove these toxic azo dyes from the industrial wastewater has become a topic of great interest. Adsorption is considered as an alternative method to the traditional combination of chemical and biological processes for the removal of dyes from aqueous solutions.[4,5] Dye adsorption by various adsorbents is considered to occur primarily via π interaction, hydrogen bonding, and electrostatic interactions. Several organic and inorganic materials including zeolite,[2,6] lignocellulosic substrate,[7,8] activated carbon,[9] graphite,[10] and graphene oxide have been all tested and shown to have different adsorption activities toward organic dyes in wastewater.[11,12] Some of these adsorbents have a rather high dye-removal efficiency; however, low-cost renewable green bioadsorbents are still rare for this field of application, and further studies are urgently required.[13]

The biorefinery concept has received considerable attention in the last decade because of advances in biotechnology and

Received: November 2, 2019
Accepted: January 23, 2020
Published: February 6, 2020

https://dx.doi.org/10.1021/acsomega.9b03717
ACS Omega 2020, 5, 2865−2877

genetic engineering, offering a renewable and sustainable alternative to the production of common petrochemicals.[14] Abundant lignocellulosic biomass is a second-generation nonfood feedstock that, when used by future biorefineries, has the potential to significantly offset the carbon footprint of the traditional refining.[15] As one of the most important renewable fractions found in biomass, lignin is still significantly underutilized in the current biorefinery industries, which has mainly focused on transforming biomass carbohydrates to liquid fuels.[16] It is anticipated that with the growing demand of biomass for production of fuels, the production of lignin would also substantially increase, potentially serving as a versatile platform for the production of biopolymers and renewable high-performance materials. The Renewable Fuel Standard (RFS) established in 2005 and further expanded in 2007 by the Energy Independence and Security Act (EISA) aims to ascend to 36 billion gallons of renewable fuel in 2022. Assuming a yield of 335 L per dry Mg of biomass, 223 million Mg of biomass will be used annually, producing about 62 million Mg of lignin.[17] To avoid using lignin as a low-grade boiler fuel, new thermal and chemical processes are needed to generate value-added products from lignin.

A lignin macromolecule contains various amounts of functional groups including carbonyl, methoxy, carboxyl, and hydroxyl groups, which offers promising opportunities to take advantage of its versatile functionality for multiple applications.[18] Without any further chemical treatments, lignin could be directly incorporated into a polymeric matrix to be served as an antioxidant,[19] a flame retardant,[20] dye adsorbent,[21,22] and a UV stabilizer.[23] Given the diversity of lignin, variability in performance as a functionalized polymer is expected to depend on the plant sources, lignin isolation methods, and physicochemical structures of lignin. Thus, chemical modifications of lignin to improve its valorization have attracted growing attention.[24,25] Lignin amination refers to a process that introduces an amine group into the lignin structure. One of the bases of lignin amination is the Mannich reaction that refers to the reaction between the lignin and amine in the presence of formaldehyde. The obtained aminated lignin has properties that make it ideal for use in several applications, including surfactants,[26] dispersants,[27] heavy metal adsorbents,[28] and asphalt emulsifiers.[29,30] Because of its aromatic/phenolic nature and cationic side chain, the aminated lignin could have great potential as a low-cost bioadsorbent for the removal of organic dyes especially azo dyes that are typically anionic in charge in wastewater.

Here, we used a cosolvent enhanced lignocellulosic fractionation (CELF) method as a highly effective lignin-first pretreatment approach that is capable of extracting highly pure technical-grade lignin from corn stover. CELF applies aqueous mixture of tetrahydrofuran (THF) and dilute acid to greatly enhance the fractionation of lignin, hemicellulose, and cellulose fractions in biomass while promoting lignin fragmentation by limiting certain lignin condensation reactions typically suffered at high reaction severities. The obtained CELF lignin is depolymerized, containing lower aryl ether linkages and higher phenolic hydroxyl groups than the typical native milled wood lignin, cellulolytic enzyme lignin, or kraft lignin, which favors the subsequent amination process.[31,32] The isolated CELF lignin was then aminated by diethylenetriamine (DETA) in the presence of formaldehyde under acid conditions via the Mannich reaction. An orthogonal array system was also applied to test the optimal conditions for the Mannich reaction. The obtained final aminated lignin was thoroughly characterized by various analytical techniques including Fourier-transform infrared spectroscopy (FTIR), nuclear magnetic resonance spectroscopy (NMR), scanning electron microscopy (SEM), thermal gravimetric analysis (TGA), and Brunauer–Emmett–Teller (BET) surface area analysis. Finally, the performance of the obtained aminated CELF lignin as a biorenewable adsorbent for the removal of methylene blue (MB) and direct blue (DB) dyes was evaluated and compared to other reported adsorbents from literature. The combinatorial process takes advantage of the selectivity of the Mannich chemistry and the unique versatile functionality of CELF lignin such as low ether linkages and high phenolic OH content. It is fully expected that this study will provide a baseline for future studies to synthesize a renewable lignin-based dye adsorbent in advanced wastewater treatment systems.

RESULTS AND DISCUSSION

Synthesis and Characterization of Adsorbents. *Orthogonal Experiments.* Systematic experimental designs such as response surface methodology and orthogonal arrays are widely used to obtain the optimal response.[33,34] An orthogonal experiment design (L16, 5^4) including five factors (A: temperature, B: time, C: amine content, D: formaldehyde content, and E: acetic acid content) at four different levels was first applied to determine the optimal Mannich reaction conditions. The Mannich reaction can only occur between a high electron density carbon and an immonium ion formed from formaldehyde and an amine, thus the amine groups are expected to be introduced only at the ortho or para position of a phenolic hydroxyl group, converting H or G types of free phenolic hydroxyl group (or both) to C_5 substituted hydroxyl groups (Figure 1).[35] This provides a unique opportunity to

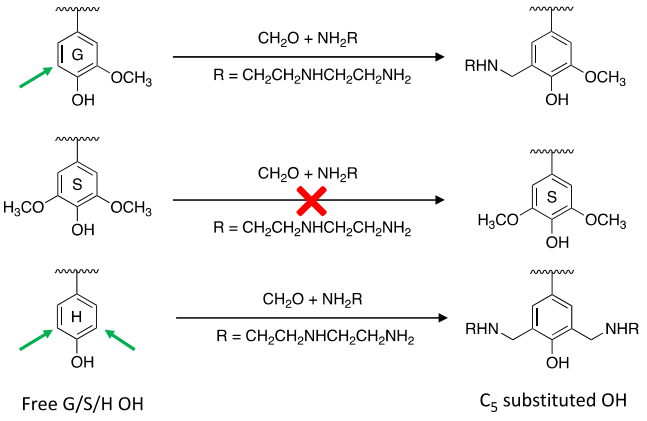

Figure 1. Mannich reaction between the phenolic G/S/H lignin and DETA, leading to the formation of phenolic C_5 substituted lignin units.

determine the extent of lignin amination by tracking the content of free H and G phenolic hydroxyl groups. Quantitative ^{31}P NMR technique was used to track the content of free H and G phenolic hydroxyl groups, aiming to assess the extent of lignin amination. Table 1 shows the conversion of H and G types of free phenolic hydroxyl for each experiment of the designed orthogonal array. As indicated by Table 1, the effect of each experiment parameter on the extent of lignin amination increases in this order: acetic acid content (E) < reaction time (B) < DETA content (C) < formaldehyde

https://dx.doi.org/10.1021/acsomega.9b03717
ACS Omega 2020, 5, 2865−2877

Table 1. L_{16} (P5)[L4] Orthogonal Experiment Design of the Mannich Reaction between CELF Lignin and DETA under Acid Conditions[a]

experiment[b]	temp. (A)	time (B)	DETA (C)	formal. (D)	acid (E)	(G + H) phenolic conversion (%)
1	A1	B1	C1	D1	E1	43.8
2	A1	B2	C2	D2	E2	46.9
3	A1	B3	C3	D3	E3	52.5
4	A1	B4	C4	D4	E4	55.6
5	A2	B1	C2	D3	E4	57.1
6	A2	B2	C1	D4	E3	81.0
7	A2	B3	C4	D1	E2	59.4
8	A2	B4	C3	D2	E1	61.1
9	A3	B1	C3	D4	E2	84.3
10	A3	B2	C4	D3	E1	85.0
11	A3	B3	C1	D2	E4	89.8
12	A3	B4	C2	D1	E3	77.1
13	A4	B1	C4	D2	E3	48.9
14	A4	B2	C3	D1	E4	63.4
15	A4	B3	C2	D4	E1	78.3
16	A4	B4	C1	D3	E2	90.8
*K*1[c]	49.7	58.5	76.3	60.9	67.0	
*K*2	64.6	69.1	64.9	61.7	70.3	
*K*3	84.0	70.0	65.3	71.3	64.9	
*K*4	70.4	71.1	62.2	74.8	66.4	
R[d]	34.3	11.6	13.1	13.9	2.1	
best quality level	A3	B4	C1	D4	E2	
optimal combination	**75 °C, 4 h, 4 mmol DETA, 16 mmol formal aldehyde, 0.2 mL acetic acid**					

[a]For each run, 200 mg of lignin was dissolved in 2 mL of dioxane. [b]Temperature A1−A4: 45, 60, 75, and 90 °C; time B1−B4: 1, 2, 3, and 4 h; DETA content C1−C4: 4, 8, 12, and 16 mmol; formaldehyde content D1−D4: 4, 8, 12, and 16 mmol; acetic acid content E1−E4: 0.1, 0.2, 0.3, and 0.4 mL. [c]*K*: average value of each factor at different levels. [d]*R*: extremum of each factor.

content (D) < reaction temperature (A), according to the extremum of each factor (*R* value). The reaction temperature was found to be the most important factor, and the extent of amination appears to achieve its maximum at 75 °C. This could be because the Mannich reaction is an endothermic reaction thus it can be promoted by increasing the temperature. A further increase in temperature has been shown to have a negative effect on animation, which could be because of unnecessary formaldehyde and DETA evaporation, thus resulting in a decrease of reaction efficiency.[36] In conclusion, the optimal combination parameters of the experiment are 75 °C, 4 h, 4 mmol DETA, 16 mmol formaldehyde, and 0.20 mL acetic acid, according to the average values of each factor at different levels (*K* value). A large scale batch reaction was then performed at this optimal condition, and the obtained aminated CELF lignin was subsequently characterized by several state-of-the-art analytical techniques.

FTIR Analysis. The structural characteristics of the CELF lignin and aminated lignin were analyzed by FTIR as shown in Figure 2. Results showed that the aminated CELF lignin exhibited some basic adsorption peaks of CELF lignin, which indicates that the skeleton structure of lignin remains basically intact during the Mannich reaction. For example, hydroxyl group stretch (3400 cm^{-1}), asymmetrical stretching vibrations of $-CH_3$ and $-CH_2-$ (2937 cm^{-1}), and symmetrical

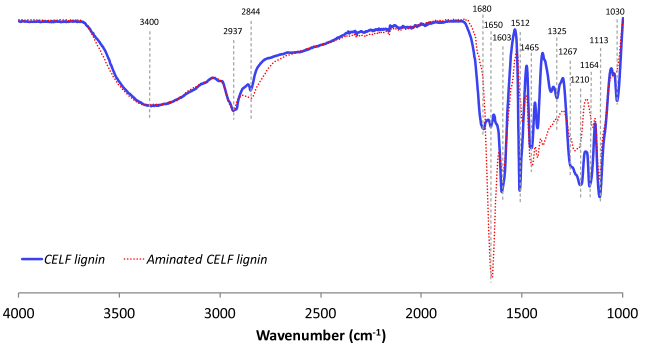

Figure 2. FTIR spectra of the corn stover CELF lignin and aminated CELF lignin.

stretching vibrations of $-CH_3$ and $-CH_2-$ (2844 cm^{-1}) are observed in both lignin samples. Nonetheless, there exist obvious differences between the lignin and aminated lignin samples. For example, the intensity of FTIR peaks associated with the aromatic C−H vibrations including 1603 and 1512 cm^{-1} from the aminated lignin is significantly lower than that from the original CELF lignin. This is because the Mannich reaction mainly occurred in the aromatic region of lignin.[37] In addition, the intensity of FTIR peaks associated with G units including 1267 cm^{-1} (C−O stretch), 1113 cm^{-1} (deformation vibrations of C−H), and 1030 cm^{-1} (aromatic C−H in-plane deformation) and H units such as 1164 cm^{-1} (C−O stretch) is decreased after amination reaction.[38] On the other hand, the intensity of syringyl C−O stretch (1325 cm^{-1}) remains relatively strong after Mannich reaction.[38] This is because the amine group could be only introduced at the C_3 or C_5 position of H lignin and the C_5 position of the G units. Finally, a strong peak around 1650 cm^{-1} representing the N−H bending vibrations in the amine structure (NH_2) appeared in the aminated lignin, validating the successful addition of the amine.[39] The peak of carbonyl group around 1680 cm^{-1} also disappears after Mannich reaction possibly because of the reaction between C═O and primary amines to form imine derivatives known as Schiff bases.[40]

2D HSQC Analysis. Two-dimensional HSQC NMR has been comprehensively used in lignin characterization because of its versatility in offering structural insight into the lignin subunits and interlinkages.[41] The reaction mechanism of Mannich reaction and the chemical structural transformation of CELF lignin during the amination reaction was further characterized by 2D HSQC NMR in this study. As shown in Figure 3, the CELF lignin possesses typical structural aromatic patterns of corn stover lignin. Peaks related to S, G, H, *p*-coumaric acid (*p*CA), ferulic acid (FA), and tricin (T) are all well defined in the aromatic region.[42] Condensed S and G signals were also found in the CELF lignin, which are commonly observed from the lignin isolated by cosolvent pretreatment at temperature conditions of 180 °C or higher with acid.[43−45] However, there exist dramatic differences between the original CELF lignin and modified lignin in both the aromatic and aliphatic regions. Specifically, it was found that the cross peaks associated with G and H lignin units were significantly altered during the Mannich reaction, while the signal of the S lignin units remained relatively stable. In addition, there are two Mannich reactive sites in tricin namely T_6 and T_8, which also disappeared in the aminated lignin because of the reaction of DETA and formaldehyde at these activate aromatic sites. Several intense signals were observed in

https://dx.doi.org/10.1021/acsomega.9b03717
ACS Omega 2020, 5, 2865−2877

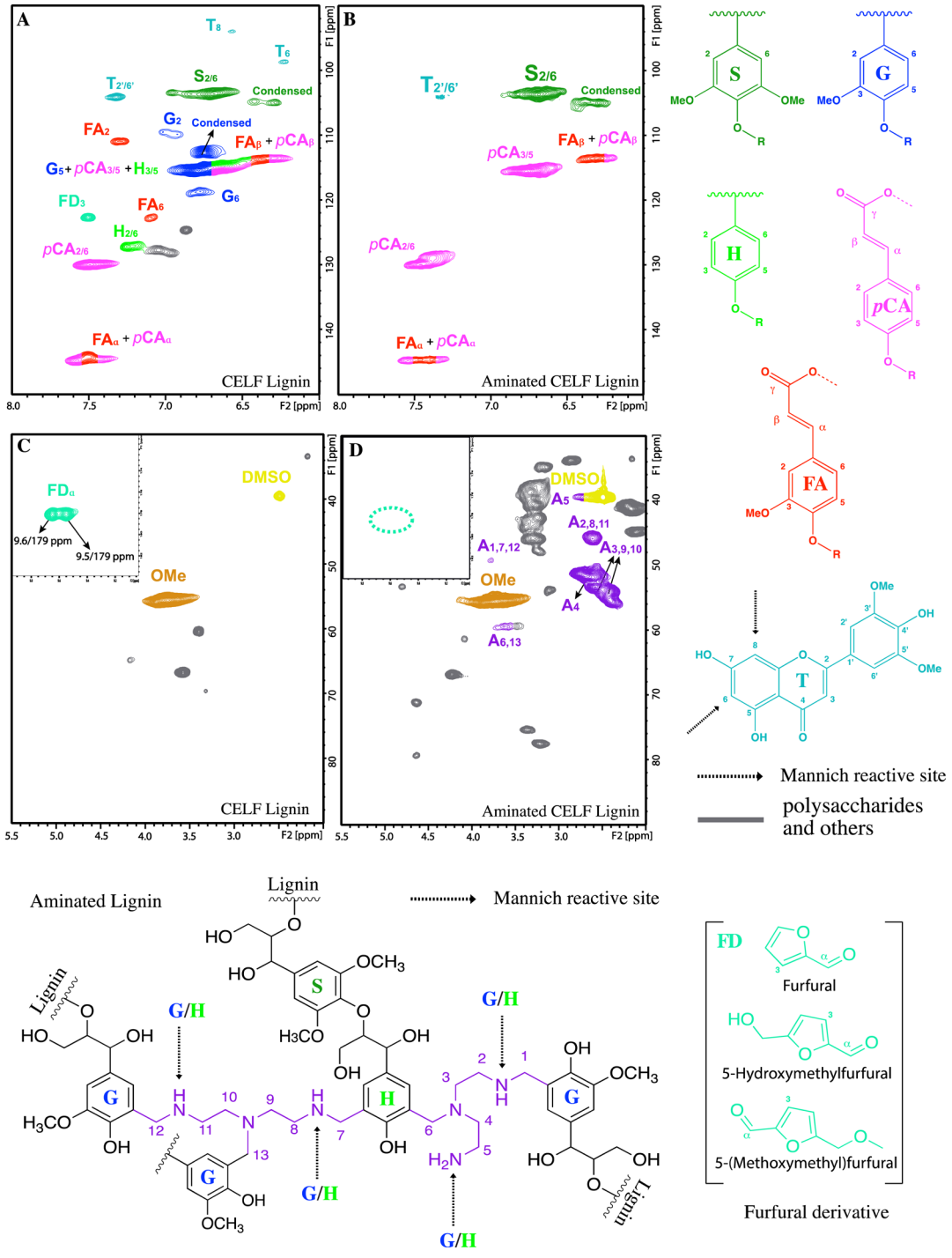

Figure 3. HSQC analysis of the original CELF lignin and its aminated product. (A) CELF lignin aromatic region; (B) aminated lignin aromatic region; (C) CELF lignin aliphatic region; (D) aminated lignin aliphatic region.

the CELF lignin at δ_C/δ_H 178/9.5−9.6 ppm and δ_C/δ_H 123/7.5 ppm, representing the aldehyde (C_α) and furanic C−H (C_3) signals of the five-substituted furfural derivatives, respectively.[41] It has been reported that these types of furfural derivatives such as 5-hydroxymethyfurfural or 5-(methoxymethyl)furfural, which arose from sugar dehydration reactions could be condensed with the lignin structure during the acid catalyzed organosolv pretreatments.[46] These types of structure were absent after the Mannich reaction possibly because of the reaction between aldehydes and primary amines to form Schiff bases.[40]

In the aliphatic region, lignin interlinkages especially the β−O−4 linkages were dramatically cleaved during the CELF pretreatment process, and in fact, these linkages could be only detected at a noise level (data not shown). This is consistent with previous studies that reported CELF pretreatment performed at high severities (180 °C) was capable of achieving near-complete removal of its native β-aryl ether linkages without hydrogen input or further heterogeneous catalytic processing.[31,47] This process is expected to generate a substantial amount of phenolic hydroxyl groups that favor the subsequent amination process. The methoxyl group

https://dx.doi.org/10.1021/acsomega.9b03717
ACS Omega 2020, 5, 2865−2877

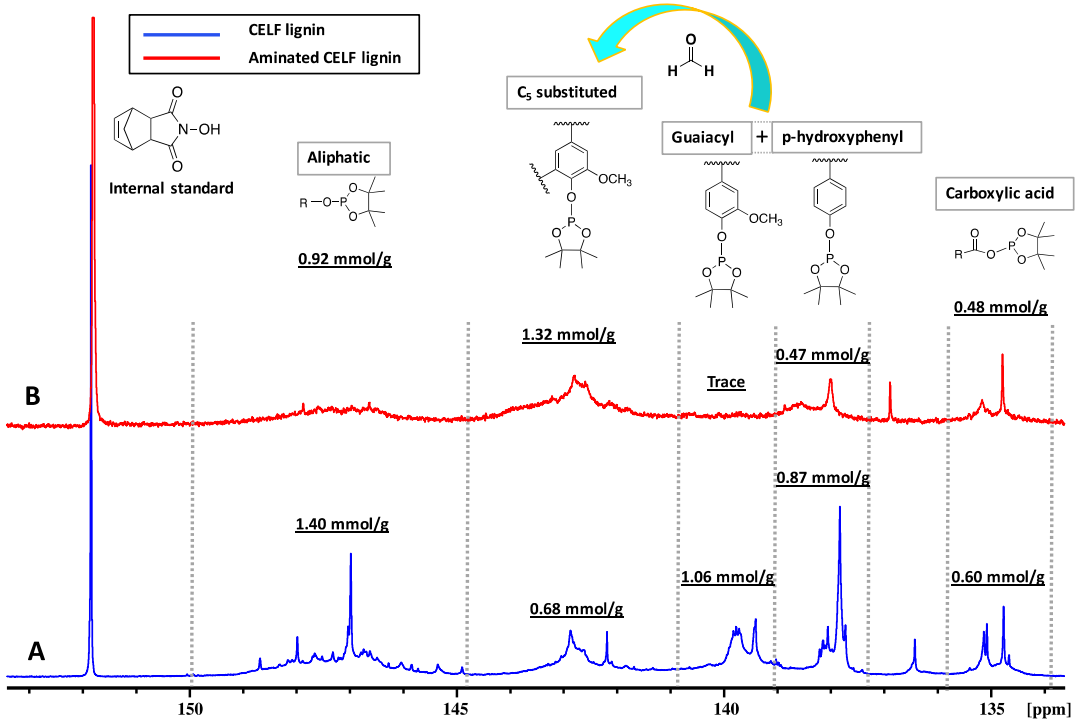

Figure 4. Quantitative ^{31}P NMR spectra of the (A) CELF lignin and (B) aminated lignin.

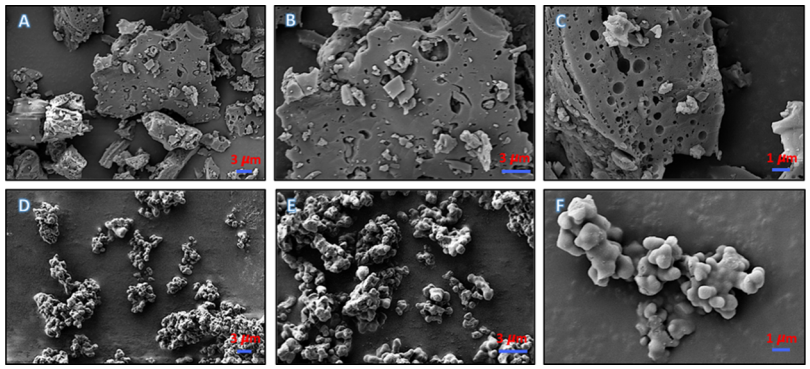

Figure 5. SEM images of lignin (top) and aminated lignin (bottom). (A,D): Mag. = 5k; (B,E): Mag. = 10k; (C,F): Mag. = 20k.

remains as the pronounced functional group in both lignin spectra. Compared to the unmodified CELF lignin, a significant amount of new signals appeared in the phenolic lignin side chain of aminated lignin, which was mainly ascribed to the methylene bridge of DETA introduced during the Mannich reaction. Our HSQC analysis also reveals that both the primary and secondary amines are capable of activating the formaldehyde. As shown in Figure 3, there still exist plenty of secondary amines in our proposed aminated lignin structure, which means that as new formaldehyde is activated by these protons, additional reactive phenolic G and H units could be subsequently grafted onto these partially aminated lignins until all the protons on the N atoms are replaced. A schematic diagram of Mannich reaction and the structural transformation of CELF lignin during the amination reaction is shown in Figure S3. The unmodified and aminated lignin was also subjected to a qualitatively visual ninhydrin test (Figure S4). The original CELF lignin had a negative/orange color indicating the absence of amines, while the change of color in the aminated lignin proved the existence of primary and secondary amine groups.

^{31}P NMR Analysis. Quantitative ^{31}P NMR technique was further employed to determine different types of hydroxyl groups including aliphatic, phenolic, and carboxylic acid in the CELF lignin and aminated lignin, and the results are shown in Figure 4. The phosphitylation reaction of various OHs in lignin structural units with TMDP is shown in Figure S5. According to a recent study, the S hydroxyl group and condensed G hydroxyl groups are not fully baseline resolved and therefore are combined into C_5 substituted hydroxyl groups in this study to avoid any possible overestimation of S and underestimation of the G condensed unit.[48] As compared to the original CELF lignin, a noticeable decrease in phenolic G and H hydroxyl groups was observed in the aminated CELF lignin after Mannich reaction. By contrast, the content of phenolic C_5 substituted hydroxyl groups including the S and condensed G and H units were considerably higher in the modified lignin than that in the original CELF lignin. The ^{31}P results also indicated that the reactivity of the reaction sites in G lignin units was higher than that in the H lignin, and as a result, the proportion of the G unit decreased more obviously than the H unit. The slight loss of aliphatic hydroxyl group may result

https://dx.doi.org/10.1021/acsomega.9b03717
ACS Omega 2020, 5, 2865−2877

from the possible loss of hydrophilic lignin fragment during the dialysis of aminated lignin.

SEM Analysis. The modified lignin sample was obtained by rotatory evaporation and centrifugation followed by extended dialysis and freeze-drying. After repeated vacuum evaporation and centrifugation, the formation of a turbid suspension suggested the possible presence of aminated lignin nanoparticles. The morphological changes of CELF lignin during Mannich reaction are monitored by SEM and displayed in Figure 5. The unmodified CELF lignin in the solid state has a much larger particle size compared to the aminated lignin and appears granulated with irregular grains of compact structure. The surface of aminated lignin is much smoother than that of the original lignin. The nanospheric particles also aggregated into a micron-sized cluster with undefined shapes in the aminated lignin, which were possibly induced by the freeze-drying process.[49]

Thermal Gravimetric Analysis. The first derivative of the thermogravimetric (DTG) curves of the original CELF lignin and its aminated products exhibited different thermal degradation stages in N_2 (Figure 6). Overall, the aminated

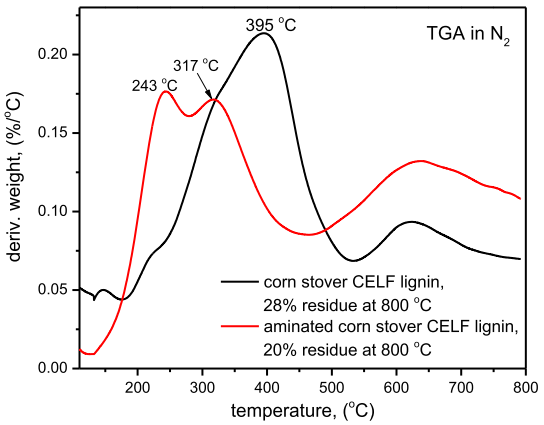

Figure 6. Derivative thermogravimetric curves of the CELF lignin and aminated lignin.

CELF lignin degraded faster than the unmodified lignin. In the pyrolysis range (200−600 °C), the DTG curve for the CELF lignin exhibits a single decomposition step with a decomposition peak temperature of 395 °C, while the curve for the aminated CELF lignin exhibits two composition steps, which are around 243 and 317 °C. The decomposition step above 300 °C is probably because of the cleavage of the C−C linkages and the demethoxylation of aromatic ring.[37,50] The lower degradation temperature for aminated lignin is probably because of the lower C−N bond energy compared to the C−C bond. The decomposition step around 243 °C could be because of the degradation and evaporation of small molecular weight lignin fragments such as aliphatic side chains. The final degradation step around 600 °C is probably because of the crack of C−C/H bond of the charcoal that was formed during the pyrolysis.[51]

BET Surface Area Analysis. Table 2 summarizes the BET specific surface areas (S_{BET}) and Barrett−Joyner−Halenda (BJH) pore volumes (V_{BJH}) of the lignins before and after amination. Results indicated that the aminated lignin exhibited higher S_{BET} and V_{BJH} than those of the original CELF lignin. For example, the S_{BET} values were 4.2 and 5.9 m^2/g for the CELF lignin and aminated lignin, respectively. In addition, the

Table 2. Surface Area and Pore Volume of the CELF Lignin and Aminated Lignin as Determined by Physisorption Analysis

sample	BET surface area (m^2/g)	BJH pore volume (cm^3/g)
CELF lignin	4.2	0.002
aminated CELF lignin	5.9	0.006

mesoporosity of these lignin samples is also confirmed by the pore size distribution analysis (Figure S6). Because the aminated lignin had a larger surface area, it provided more adsorption sites, and hence enhanced dye removal can be anticipated.

Removal of Dye by the Adsorbent. To demonstrate the potential dye-adsorption property of the modified CELF lignin, two types of dyes were tested in the lignin-dye adsorption experiment: a cationic dye MB and an anionic azo dye DB 1. The qualitative and quantitative effect of lignin loading on the dye decolorization efficiency for the original and aminated lignin is shown in Figure 7. These results indicated that the aminated lignin showed drastically improved decolorization efficiency for both dyes especially the anionic DB 1 dye. For example, the amination process increased the DB 1 dye-removal efficiency from <5 to >90% even at extremely low lignin loadings. The decolorization efficiency for MB dye is proportional to the dose of lignin, while no correlation could be obtained between the efficiency of DB 1 dye removal and the concentration of lignin. This might be attributed to the unmodified lignin inability to adsorb DB 1 dye even at extremely high lignin dose and the aminated lignin strong ability to adsorb DB 1 dye even at low lignin loadings. The effect of amino content on the adsorptivity of the aminated CELF lignin was further investigated, and the results indicated that the dye decolorization efficiency was positively correlated to the amino content of the modified CELF lignin (Figure S7). The modified lignin has much higher decolorization efficiency toward the anionic dye (DB 1) compared to the cationic dye (MB). This could be mainly because of the electrostatic coupling between the cationic side chain (amine group) of the aminated lignin and the anionic sites of the DB 1 dye.[52] It is well known that pH affects the adsorption of most organic pollutants as well as the surface charges of adsorbents. To further confirm that electrostatic interactions are key mechanism of adsorptive removal of dyes in DB 1 dye in aqueous solutions, the effect of initial pH on the dye decolorization efficiency and zeta potential of aminated CELF lignin was evaluated within the pH range of ∼4.0 and 10.0 (Figure 8). At extreme acidic or basic conditions (pH < 3 or > 12), lignin samples were found to be partially or completely dissolved in aqueous solutions, thus their adsorption and surface charge behaviors were not investigated at these conditions. These results also indicated that high pH values resulted in a decrease in the adsorptivity of aminated CELF lignin, which could be because of the increase of the magnitude of the negative zeta potential as pH increases. The aminated CELF lignin has a point of zero charge (pH_{PZC}) around 4.5, and its magnitude of zeta potential at each tested pH value (−2 to −25 mV) is significantly lower than that of the unmodified CELF lignin ranging from −68 to −75 mV (Figure 8). This is because of the addition of the cationic amine group onto the side chain of aminated lignin. DB 1 dye has four sulfonate groups, thus it remains negatively charged at

https://dx.doi.org/10.1021/acsomega.9b03717
ACS Omega 2020, 5, 2865−2877

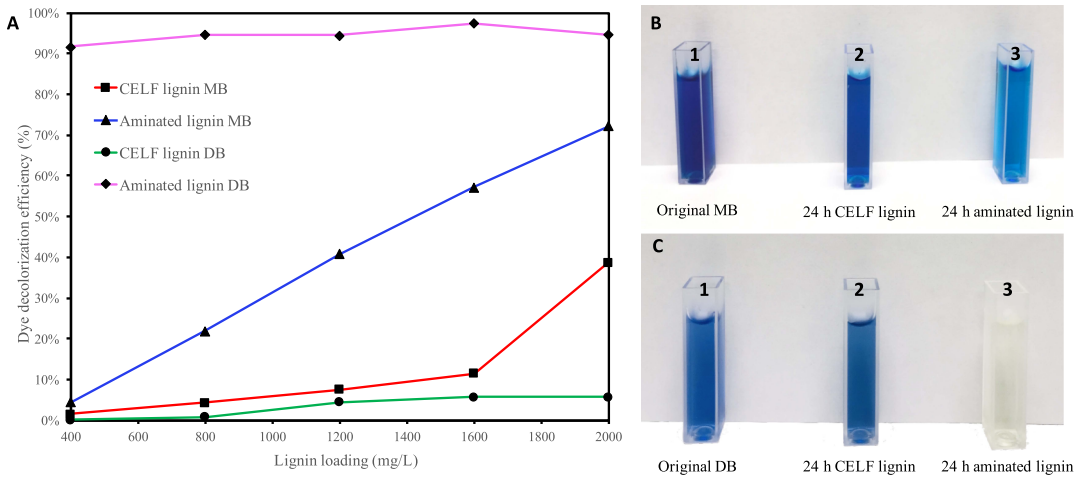

Figure 7. Dye adsorption capacity of the CELF lignin and aminated lignin. (A) Effect of lignin loading on dye decolorization efficiency. (B) MB dye before (1) and after (2, 3) 24 h lignin adsorption. (C). DB 1 dye before (1) and after (2, 3) 24 h lignin adsorption.

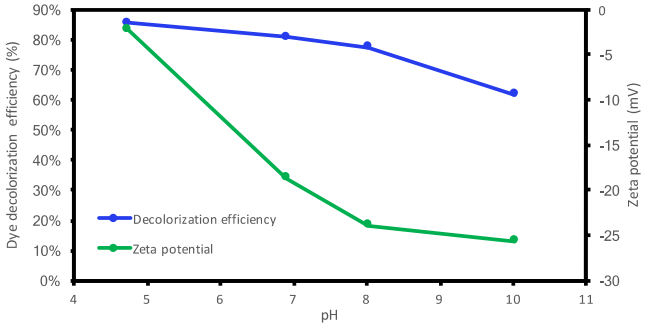

Figure 8. Effect of pH on the zeta potential and adsorptivity of the modified lignin toward DB.

basic conditions and even at highly acidic solutions as these protonated sulfonate groups have a pK_a value lower than zero.[53] Therefore, the increase of the net negative zeta potential could further cause a decrease of the electrostatic interactions between the cationic lignin side chain and the negatively charged DB 1 dye in aqueous solution. This suggests that electrostatic force is a major interaction for DB 1 dye adsorption at lower pH. Furthermore, the decolorization efficiency is still above 60% even at high pH, although there exists substantial electrostatic repulsion between the modified lignin and DB 1 dye. This indicates that mechanisms other than electrostatic interaction such as hydrogen bonding and $\pi-\pi$ stacking are also operative for the DB 1 dye adsorption on the aminated CELF lignin.[54] On the other hand, hydrogen bonding, π-interaction, and limited electrostatic interaction between lignin dissociated carboxyl/hydroxyl groups and the cationic sites of the dye molecule are believed to be responsible for the MB dye adsorption.[1] Figure 9 shows a proposed scheme for the MB and DB 1 dye binding to the unmodified CELF lignin and aminated lignin surface.

The Langmuir and Freundlich model was used to study the adsorption isotherms of azo-dyes, and their equations (eqs 1 and 2) are shown below

$$\frac{C_e}{Q_e} = \frac{C_e}{Q_m} + \frac{1}{Q_m K_L} \quad (1)$$

$$\log Q_e = \log K_F + \frac{1}{n}\log C_e \quad (2)$$

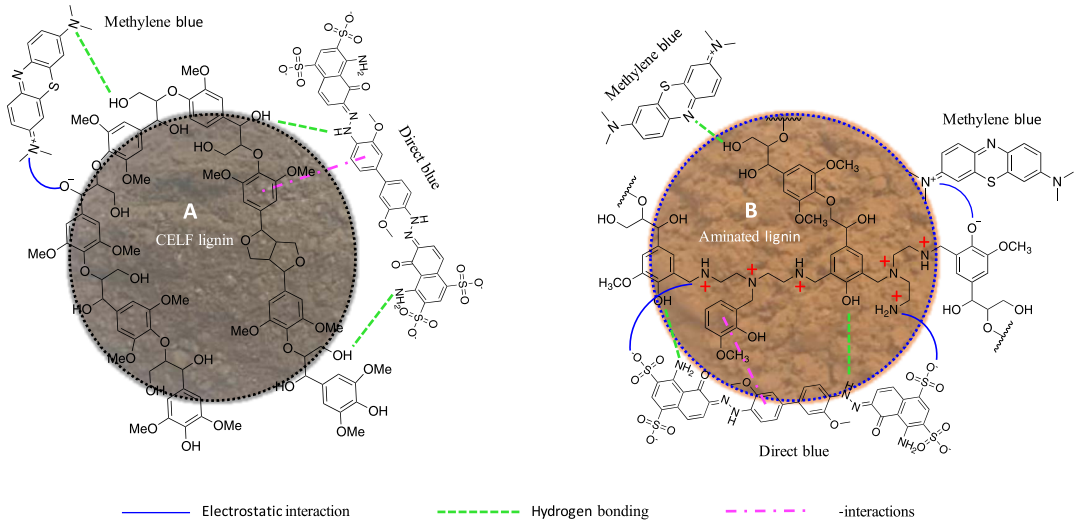

Figure 9. Proposed scheme of DB and MB dye binding to the CELF lignin (A) and aminated lignin (B).

https://dx.doi.org/10.1021/acsomega.9b03717
ACS Omega 2020, 5, 2865−2877

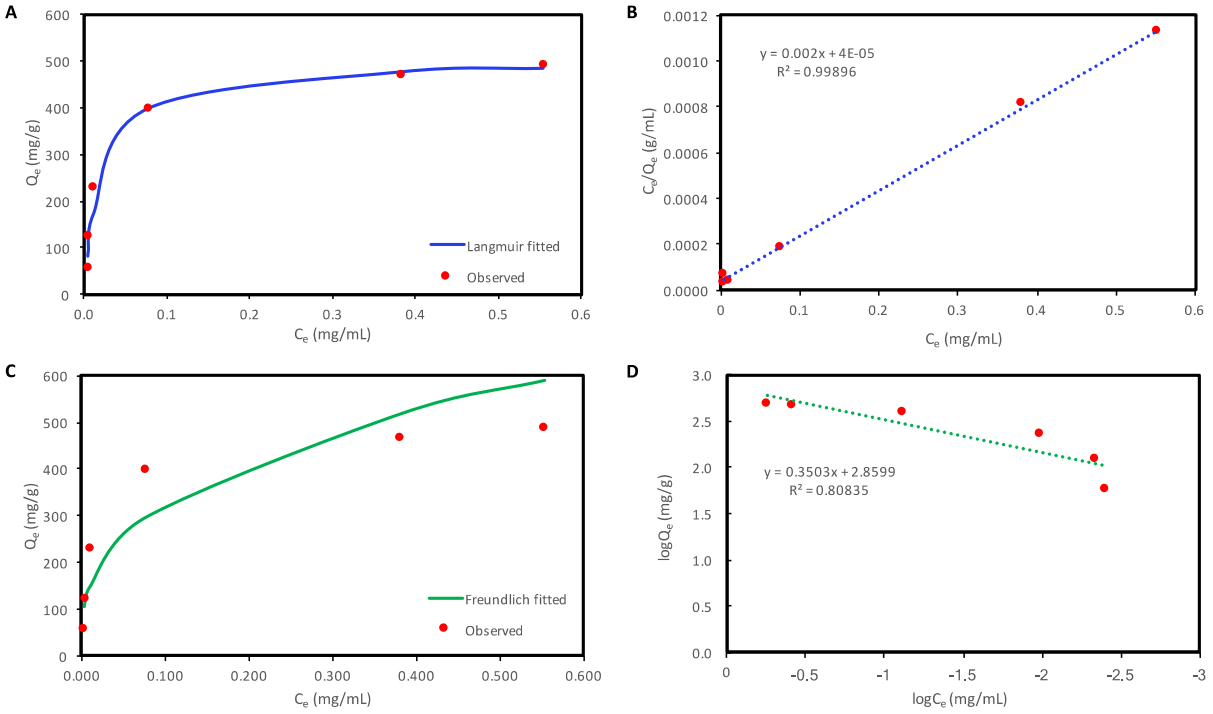

Figure 10. Adsorption isotherms of DB 1 by aminated CELF lignin. (A) Langmuir fitted adsorption isotherm curve; (B) linear fit of the Langmuir model (R^2 = 0.99); (C) Freundlich fitted adsorption isotherm curve; (D) linear fit of the La Freundlich model (R^2 = 0.81).

where c_e (mg/mL) is the equilibrium concentration, Q_e (mg/g) is the equilibrium adsorption capacity, Q_m (mg/g) is the maximum adsorption capacity of the Langmuir isotherm model, K_L (mL/mg) is a Langmuir adsorption coefficient, K_F (mL/mg) is the Freundlich constant, and $1/n$ is an indicator that reflects the nonlinear degree of adsorption. Figure 10 shows the Langmuir (A) and Freundlich (C) adsorption isotherms curves, and the linear analysis (B and D) indicated that the observed dye adsorption data for aminated CELF lignin were better described by the Langmuir isotherm model as confirmed by the higher coefficient R^2. The Langmuir fitting results suggested that the adsorption process between the lignin and the azo dye could be characterized as a monolayer type of adsorption. The Langmuir isotherm analysis indicated that the maximum adsorption capacity of the aminated CELF lignin is 502.7 mg/g for DB 1 dye. A direct comparison of the maximum adsorption capacities of different anionic azo dyes on various previously reported adsorbents is presented in Table 3. Based on our literature survey, it was found that the adsorption capacity of aminated CELF lignin is higher than that of all other adsorbents except carbon nanospheres. It should be noted that these adsorbents include commercial activated carbon, anion exchange membrane, and multiwalled carbon nanotubes, which are all well-known for their high aspect ratio, natural porosity, and strong ability to adsorb pollutants from the aqueous system. This suggests that the aminated CELF lignin, as a low-cost renewable resource, is highly suitable for the removal of azo-dyes from the aqueous solutions.

The rate of the adsorption process is an important factor that determines if the sorbent could be used on large scales in industrial applications and it can be determined by kinetic studies. In the study of solid−liquid static adsorption kinetics, the relationship between the time and the amount of adsorption is typically fitted through dynamic models.[64] Two

Table 3. Adsorption Performance of Different Adsorbents toward Azo-Dyes as Characterized by the Maximum Adsorption Capacity (mg dye/g Substrate)

adsorbent	dye adsorbate	maximum capacity (mg/g)	references
granular activated carbon	Congo red	9.1	55
zeolite	DB 71	13.7	6
graphene oxide	acid orange 8	29.0	11
chitosan halloysite nanotubes	Congo red	41.5	56
multiwalled carbon nanotube	tartrazine	84.0	57
$Mn_{0.4}Zn_{0.6}Fe_2O_4$ nanoparticles	tartrazine	90.8	58
$Mn_{0.4}Zn_{0.6}Fe_2O_4$ nanoparticles	Ponceau 4R	101.4	58
SEG-modified starch	direct red 23	129.9	59
SEG-modified starch	acid blue 92	147.1	59
lignin amine-coated Fe_3O_4	acid scarlet GR	176.5	54
chitosan	tartrazine	350	60
multiwalled carbon nanotube	DB 53	409.4	53
graphene oxide sponge	direct red 80	501.3	5
aminated CELF lignin	***DB 1***	***502.7***	***present***
chitosan-based hydrogel	erichrome black T	520	61
carbon nanospheres	acid red 88	555.6	62
$Fe(OH)_3$@cellulose hybrid fibers	Congo red	689.7	63

mathematical models are usually adapted to analyze the dynamic models of adsorption process, namely pseudo-first-order (eq 3) and pseudo-second-order (eq 4) equation

$$\log(Q_e - Q_t) = \log Q_e - \frac{K_1 t}{2.303} \quad (3)$$

https://dx.doi.org/10.1021/acsomega.9b03717
ACS Omega 2020, 5, 2865−2877

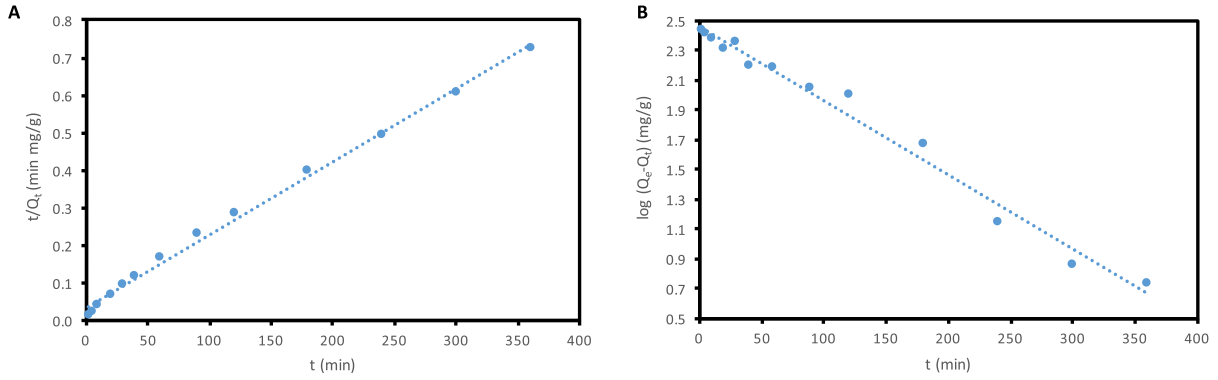

Figure 11. Pseudo-second-order plot (A) and pseudo-first order plot (B) for the DB dye adsorption kinetics by the aminated CELF lignin.

$$\frac{t}{Q_t} = \frac{t}{Q_e} + \frac{1}{Q_e^2 K_2} \quad (4)$$

where Q_e and Q_t are adsorption capacity (mg/g) at equilibrium time and any instant of adsorption time t (min) and K_1 and K_2 are the rate constant of the pseudo-first-order and second-order adsorption, respectively. The study about the effect of time on the adsorption process, as shown in Figure S8, suggests that the amount of dye adsorbed by the adsorbent increases rapidly at the beginning for 30 min, and then the adsorption efficiency becomes slow for 240 min until the adsorption equilibrium is reached. The pseudo first and second kinetic models assume that the adsorption process is governed by diffusion and chemical adsorption mechanism, respectively. The observed experimental data were fitted to the pseudo-first-order and second-order equations, and their linear fitted plots and the parameters of the kinetic model are shown in Figure 11 and Table 4, respectively. It was found that the correlation

Table 4. Parameters of the Adsorption Kinetic Model

kinect model	q_e (mg g^{-1})	K_1 (min^{-1}) or K_2 (g mg^{-1} min^{-1})	R^2
pseudo-first order	285.8	0.01152	0.984
pseudo-second order	511.7	0.00013	0.996

coefficient (R^2) of pseudo-second-order equation kinetic model was higher than that of the pseudo-first-order model, suggesting that the pseudo-second-order kinetic model may be more suitable for describing the kinetics of the adsorption process of the DB 1 dye on the aminated CELF lignin. This suggested that the adsorption behaviors of azo-dye onto the modified lignin are dominated by chemical adsorption instead of diffusion process. It has been reported that the adsorption process is generally divided into three main stages, including the film diffusion stage, intraparticle diffusion stage, and the final actual adsorption stage.[65] To further test if the intraparticle diffusion is the only rate determining step of the adsorption process, the intraparticle diffusion kinetic model is also fitted with the experimental data (Figure S9), and results indicated that the adsorption process has more than one speed-controlling step. In addition, the relatively large boundary layer thickness as reflected by the large intercept of the linear plot ($t^{1/2}$ vs q_t) suggests that membrane diffusion might also have a great effect on the adsorption process.[65]

Reusability of the adsorbent represents an important aspect to minimize the cost of the overall adsorption process. The recycle performances of aminated CELF lignin for DB 1 dye removal were also investigated in this study. The results, as shown in Figure 12, show that no significant reduction in the

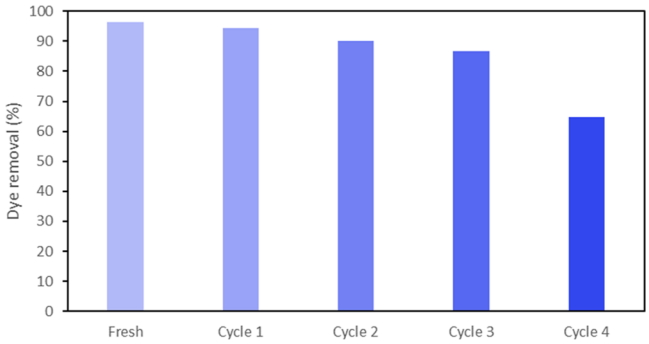

Figure 12. Removal efficiency of the aminated CELF lignin for DB 1 dye after four adsorption−desorption cycles.

adsorption efficiency is found for three cycles compared with that of the fresh adsorbent, although there is a gradual decrease in the dye-removal efficiencies possibly because of the incomplete of dye desorption. The dye-removal efficiency decreased to 65% for the fourth use, probably because of the saturation of the adsorbent surface. Thus, the recycle study demonstrated that the aminated CLEF lignin remained as an efficient adsorbent even after multiple reuses.

Aminated CELF Lignin Characterization after Dye Adsorption. The FTIR spectra of aminated CELF lignin before and after dye adsorption are shown in Figure S10. After adsorption, two additional peaks at around 1200 and 1035 cm^{-1} representing the stretching vibration bands of the sulfonate group appear in the aminated lignin because of the attachment of the DB 1 dye. The N═N stretching vibration from DB 1 dye is unclear in the IR spectra because the direct dye is a symmetrical trans azo compound. SEM was also used to analyze the morphology of the aminated CELF lignin surface after the adsorption of DB 1 dye (Figure 13). Results showed that the shape of lignin particles did not change dramatically and remained as an aggregated cluster with irregular shapes and heterogeneous surface, but their size appeared to increase significantly after dye adsorption. These observations clearly revealed that the DB 1 dye is adsorbed on the surface of the modified CELF lignin.

https://dx.doi.org/10.1021/acsomega.9b03717
ACS Omega 2020, 5, 2865−2877

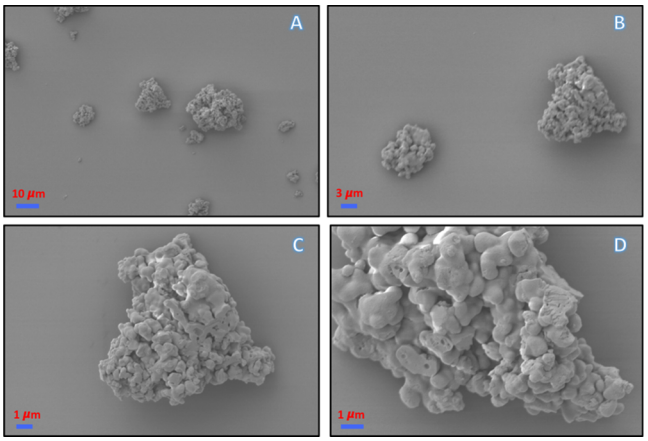

Figure 13. SEM images of the aminated lignin after adsorption of DB 1 dye. [(A) Mag. = 2k. (B) Mag. = 5k. (C) Mag. = 10k. (D) Mag. = 20k].

CONCLUSIONS

Development of low-cost renewable bioadsorbents for removal of toxic dyes from contaminated water has been a topic of great interest but remains challenging. In this study, the aminated corn stover lignin was synthesized via combinatorial CELF pretreatment and Mannich reaction to remove azo dyes from aqueous solutions. Under acid conditions, both the primary and secondary amines have high reactivity toward the $H_{3/5}$ and G_5 position of CELF lignin. SEM revealed that the original lignin particles are distributed in a large conglomerate, while the surface of aminated lignin becomes smoother, and the nanospherical particles of the modified lignin aggregate into nano- and micron-sized cluster with undefined shapes. The combination of CELF pretreatment and Mannich reaction significantly increased the adsorption behavior of aminated lignin toward azo DB 1 dye with a maximum capacity of 502.7 mg/g, which is significantly higher than that of many adsorbent materials reported in the literature. Recycle studied suggested that once recovered, the bioadsorbent was capable of maintaining a relatively high dye removal efficiency (>85%) even after three recycles. In conclusion, the proposed aminated CELF lignin could be considered as a cost-effective bioadsorptive platform for the efficient removal of azo dyes from aqueous solutions.

EXPERIMENTAL SECTION

Feedstocks and Chemicals. The Kramer corn stover was provided by the National Renewable Energy Laboratory (NREL, Golden, CO). The corn stover was knife-milled to pass through a 1 mm particle size interior sieve using a laboratory mill (model 4, Arthur H. Thomas Company, Philadelphia, PA). All the chemicals used in this study were used as received from Sigma-Aldrich without any further purification.

Production of the CELF Lignin. CELF pretreatment of corn stover was performed in a custom built 1 L Hastelloy Parr reactor (Parr instruments Company, Moline, IL) at 7.5 wt % solids loading and 0.5 wt % H_2SO_4 acid loading. The CELF reaction was sustained at 180 °C for 25 min in an equivolume mixture of THF and water. After pretreatment, the reactor was quenched in a 25 °C water bath, and the liquid phase was separated from the pretreated solids through vacuum paper filtration. The CELF lignin was then isolated from the liquid phase by first neutralization with ammonium hydroxide followed by THF evaporation and subsequent vacuum filtration of the precipitated lignin from the neutralized liquor. The obtained CELF lignin was washed with water and diethyl ether and dried at 45 °C in an incubator. Once dried, the lignin was finally crushed to a fine powder in a mortar and pestle and stored in a container prior to further test and modification.

Amination of the CELF Lignin. The corn stover CELF lignin (~200 mg) was mixed with 2 mL of dioxane in a round flask under constant stirring for 20 min at room temperature until the lignin was fully dissolved. Specified amounts of DETA, acetic acid, and formaldehyde were then added into the solution with continuous stirring. Formaldehyde was added stepwise to avoid unnecessary crosslinking reactions. Subsequently, the flask was heated in a sand bath, kept at a specified temperature (45, 60, 75, and 90 °C), and stirred for a specified time (1, 2, 3, and 4 h). Afterward, the reaction mixture was evaporated under reduced pressure to remove the majority of the organic solvent followed by dialysis with a molecular weight cut off of 1000 Da. The obtained aminated CELF lignin was finally freeze-dried and stored at room temperature before further characterization.

Lignin Characterization before and after Amination. *FTIR Analysis.* The IR spectra were collected using a Spectrum One FTIR spectrophotometer (PerkinElmer, Wellesley, MA) equipped with a diamond-composite attenuated total reflectance cell from 1000 to 4000 cm^{-1} with 128 scans at 4 cm^{-1} resolutions.

NMR Analysis. NMR experiments were acquired with a Bruker Avance III HD 500 MHz spectrometer equipped with a 5 mm N_2 cryogenically cooled BBO H&F probe, according to previously published literatures.[32,66] A standard Bruker pulse sequence (hsqcetgpspsi2.2) and an inverse-gated decoupling pulse sequence (Waltz-16) were applied for HSQC and ^{31}P NMR experiment, respectively.

SEM Analysis. The morphology of lignin samples was observed with a scanning electron microscope (Zeiss Auriga, Germany) at an accelerating voltage of 5 kV. The samples were sputter-coated with Au using an SPI-Module sputter coater for 50 s. Imaging was subsequently captured at various magnifications from 2k to 20k.

Thermal Gravimetric Analysis. The TGA was performed by a TGA Q50 thermo-gravimetric analyzer (TA instruments, UDA). Lignin samples (~5 mg) were loaded to a platinum sample pan (TA instruments) and heated in nitrogen from 25 to 105 °C at 20 °C/min. After incubating at 105 °C for 10 min, it was heated further from 105 to 800 °C at a heating rate of 20 °C/min.

Zeta Potential Analysis. The zeta potential of lignin suspensions was measured at different hydrogen ion concentrations while keeping a concentration of 1 mg/mL, using ZetaPALS (Brookhaven Instruments Corporation, NY). The mean zeta potential of each suspension was calculated from 10 measurements.

Surface Area and Pore Size Analysis. The N_2 adsorption−desorption measurement of samples was carried out at 77 K on a Quantachrome Autosorb iQ. The samples were first degassed at 353 K for ~17 h before being loaded into the analysis station. The pore volume and pore size distribution were determined using a BJH method. The specific surface area was calculated using BET in the P/P_0 range of 0.05−0.30.

Dye Decolorization Study. Various amounts of CELF lignin and aminated lignin were mixed with 25 mL of MB or

https://dx.doi.org/10.1021/acsomega.9b03717
ACS Omega 2020, 5, 2865−2877

DB 1 dye solution with a concentration of 50 mg/L. The mixture was left in an incubator at 25 °C and 150 rpm for 24 h. The concentration of dye in the supernatant of the solution at the equilibrium was determined by a UV spectrophotometer. The amount of dye adsorbed (q_e) by lignin substrates was calculated based on the following eq 5

$$q_e = \frac{v(C_o - C_e)}{m} \quad (5)$$

where c_o and c_e represent the initial and equilibrium concentrations of dye solution (mg/L), respectively, v is the volume of the total solution (mL), and m is the dry weight of the lignin sample (g). The maximum wavelength for MB and DB 1 dye was set at 663 and 624 nm, respectively. The extinction coefficient of MB and DB 1 dye was determined to be 149.3 and 12.3 L mol^{-1} cm^{-1} based on the Beer's law calibration (Figures S1 and S2). The decolorization efficiency (η) is defined by

$$\eta = \frac{C_o - C}{C_o} \times 100\% \quad (6)$$

where c_o represents the initial concentration, and c is the concentration of dye in the supernatant after decolorization. The adsorption isotherms of DB 1 dye onto aminated lignin were measured with varying concentrations of dye ranging from 0.05 to 1 mg/mL at 25 °C. To further investigate the kinetics of dye adsorption, the equilibrium concentrations of dye solution were measured from 5 min to 8 h after mixing 20 mg of aminated lignin with 40 mL of DB 1 with an initial concentration of 1 mg/mL. The effect of initial pH on dye adsorption was studied by mixing ∼10 mg of lignin with 25 mL of initial DB 1 dye with a concentration of 50 mg/mL at 25 °C. ∼0.1 M HNO_3 and 0.01 M of NaOH were used to adjust the pH between 4 and 10. For the recycling experiment, dilute NaOH (pH = 10) was used to release the adsorbed dye from the adsorbent. The adsorption of the dye by the regenerated lignin was repeated four times by mixing ∼20 mg of solid with 25 mL of MB or DB 1 dye solution with a concentration of 50 mg/L.

■ ASSOCIATED CONTENT

Supporting Information

The Supporting Information is available free of charge at https://pubs.acs.org/doi/10.1021/acsomega.9b03717.

Calibration curve of dyes; schematic diagram of Mannich reaction; ninhydrin test of lignin amination; phosphitylation reactions between lignin OHs and TMDP; pore size distribution of lignin samples; effect of amino content on the adsorptivity of aminated CELF lignin; effect of contact time on adsorption; intraparticle diffusion kinetic of DB 1 dye; and FTIR spectra of the aminated CELF lignin before and after dye adsorption (PDF)

■ AUTHOR INFORMATION

Corresponding Authors

Xianzhi Meng − *Department of Chemical & Biomolecular Engineering, University of Tennessee Knoxville, Knoxville, Tennessee 37996, United States;* orcid.org/0000-0003-4303-3403; Email: xmeng5@utk.edu

Arthur J. Ragauskas − *Department of Chemical & Biomolecular Engineering, University of Tennessee Knoxville, Knoxville, Tennessee 37996, United States; Biosciences Division, Oak Ridge National Laboratory, Oak Ridge, Tennessee 37831, United States; Department of Forestry, Wildlife, and Fisheries; Center for Renewable Carbon, The University of Tennessee Knoxville, Institute of Agriculture, Knoxville, Tennessee 37996, United States;* orcid.org/0000-0002-3536-554X; Email: argauskas@utk.edu

Authors

Brent Scheidemantle − *Center of Environmental and Research Technology (CE-CERT) and Department of Chemical and Environmental Engineering, Bourns College of Engineering, University of California, Riverside, California 92507, United States*

Mi Li − *Department of Chemical & Biomolecular Engineering, University of Tennessee Knoxville, Knoxville, Tennessee 37996, United States;* orcid.org/0000-0001-7523-1266

Yun-yan Wang − *Department of Forestry, Wildlife, and Fisheries; Center for Renewable Carbon, The University of Tennessee Knoxville, Institute of Agriculture, Knoxville, Tennessee 37996, United States*

Xianhui Zhao − *Chemical Sciences Division, Oak Ridge National Laboratory, Oak Ridge, Tennessee 37831, United States*

Miguel Toro-González − *Isotope and Fuel Cycle Technology Division, Oak Ridge National Laboratory, Oak Ridge, Tennessee 37831, United States*

Priyanka Singh − *Center of Environmental and Research Technology (CE-CERT) and Department of Chemical and Environmental Engineering, Bourns College of Engineering, University of California, Riverside, California 92507, United States*

Yunqiao Pu − *Biosciences Division, Oak Ridge National Laboratory, Oak Ridge, Tennessee 37831, United States*

Charles E. Wyman − *Center of Environmental and Research Technology (CE-CERT) and Department of Chemical and Environmental Engineering, Bourns College of Engineering, University of California, Riverside, California 92507, United States*

Soydan Ozcan − *Department of Mechanical, Aerospace, Biomedical Engineering, University of Tennessee, Knoxville, Tennessee 37996, United States; Manufacturing Demonstration Facility, Energy and Transportation Science Division, Oak Ridge National Laboratory, Knoxville, Tennessee 37932, United States*

Charles M. Cai − *Center of Environmental and Research Technology (CE-CERT) and Department of Chemical and Environmental Engineering, Bourns College of Engineering, University of California, Riverside, California 92507, United States;* orcid.org/0000-0002-5047-0815

Complete contact information is available at: https://pubs.acs.org/10.1021/acsomega.9b03717

Author Contributions

The experiments were performed through contributions of all the authors. All the authors have approved the final version of the manuscript.

Notes

The authors declare no competing financial interest.

https://dx.doi.org/10.1021/acsomega.9b03717
ACS Omega 2020, 5, 2865−2877

■ ACKNOWLEDGMENTS

This work is supported by "Agriculture and Food Research Initiative—Sustainable Bioenergy and Bioproducts Challenge Area" [grant no. USDA-NIFA-AFRI-006352/project accession no. 1015189] from the U.S. Department of Agriculture (USDA) National Institute of Food and Agriculture (NIFA). Facilities at UC Riverside were provided by the Bourns' College of Engineering Center for Environmental Research & Technology (CE-CERT). We also want to thank Sarah Humphries from the University of Tennessee—Knoxville for her administrative support including help us purchasing all the suppliers for the study.

■ REFERENCES

(1) Budnyak, T. M.; Aminzadeh, S.; Pylypchuk, I. V.; Sternik, D.; Tertykh, V. A.; Lindström, M. E.; Sevastyanova, O. Methylene Blue dye sorption by hybrid materials from technical lignins. *J. Environ. Chem. Eng.* **2018**, *6*, 4997−5007.

(2) Abdelhamid, H. N.; Zou, X. Template-free and room temperature synthesis of hierarchical porous zeolitic imidazolate framework nanoparticles and their dye and CO_2 sorption. *Green Chem.* **2018**, *20*, 1074−1084.

(3) Wang, S.; Kong, F.; Fatehi, P.; Hou, Q. Cationic High Molecular Weight Lignin Polymer: A Flocculant for the Removal of Anionic Azo-Dyes from Simulated Wastewater. *Molecules* **2018**, *23*, 2005.

(4) Peng, N.; Hu, D.; Zeng, J.; Li, Y.; Liang, L.; Chang, C. Superabsorbent Cellulose-Clay Nanocomposite Hydrogels for Highly Efficient Removal of Dye in Water. *ACS Sustainable Chem. Eng.* **2016**, *4*, 7217−7224.

(5) Zambare, R.; Song, X.; Bhuvana, S.; Antony Prince, J. S.; Nemade, P. Ultrafast Dye Removal Using Ionic Liquid-Graphene Oxide Sponge. *ACS Sustainable Chem. Eng.* **2017**, *5*, 6026−6035.

(6) Mirzaei, N.; Mahvi, A. H.; Hossini, H. Equilibrium and kinetics studies of Direct blue 71 adsorption from aqueous solutions using modified zeolite. *Adsorpt. Sci. Technol.* **2018**, *36*, 80−94.

(7) Sohni, S.; Hashim, R.; Nidaullah, H.; Lamaming, J.; Sulaiman, O. Chitosan/nano-lignin based composite as a new sorbent for enhanced removal of dye pollution from aqueous solutions. *Int. J. Biol. Macromol.* **2019**, *132*, 1304−1317.

(8) Zhang, L.; Lu, H.; Yu, J.; McSporran, E.; Khan, A.; Fan, Y.; Yang, Y.; Wang, Z.; Ni, Y. Preparation of High-Strength Sustainable Lignocellulose Gels and Their Applications for Antiultraviolet Weathering and Dye Removal. *ACS Sustainable Chem. Eng.* **2019**, *7*, 2998−3009.

(9) Singh, S.; Sidhu, G. K.; Singh, H. Removal of methylene blue dye using activated carbon prepared from biowaste precursor. *Indian Chem. Eng.* **2019**, *61*, 28−39.

(10) Oliveira, E. H. C. d.; Marques Fraga, D. M. d. S.; da Silva, M. P.; Fraga, T. J. M.; Carvalho, M. N.; de Luna Freire, E. M. P.; Ghislandi, M. G.; da Motta Sobrinho, M. A. Removal of toxic dyes from aqueous solution by adsorption onto highly recyclable xGnP® graphite nanoplatelets. *J. Environ. Chem. Eng.* **2019**, *7*, 103001.

(11) Konicki, W.; Aleksandrzak, M.; Moszyński, D.; Mijowska, E. Adsorption of anionic azo-dyes from aqueous solutions onto graphene oxide: Equilibrium, kinetic and thermodynamic studies. *J. Colloid Interface Sci.* **2017**, *496*, 188−200.

(12) Mahmoodi, N. M.; Ghezelbash, M.; Shabanian, M.; Aryanasab, F.; Saeb, M. R. Efficient removal of cationic dyes from colored wastewaters by dithiocarbamate-functionalized graphene oxide nanosheets: From synthesis to detailed kinetics studies. *J. Taiwan Inst. Chem. Eng.* **2017**, *81*, 239−246.

(13) Alatalo, S.-M.; Mäkilä, E.; Repo, E.; Heinonen, M.; Salonen, J.; Kukk, E.; Sillanpää, M.; Titirici, M.-M. Meso- and microporous soft templated hydrothermal carbons for dye removal from water. *Green Chem.* **2016**, *18*, 1137−1146.

(14) Ragauskas, A. J.; Williams, C. K.; Davison, B. H.; Britovsek, G.; Cairney, J.; Eckert, C. A.; Frederick, W. J., Jr.; Hallett, J. P.; Leak, D. J.; Liotta, C. L.; Mielenz, J. R.; Murphy, R.; Templer, R.; Tschaplinski, T. The path forward for biofuels and biomaterials. *Science* **2006**, *311*, 484−489.

(15) Amore, A.; Ciesielski, P. N.; Lin, C.-Y.; Salvachúa, D.; Sànchez i Nogué, V. Development of Lignocellulosic Biorefinery Technologies: Recent Advances and Current Challenges. *Aust. J. Chem.* **2016**, *69*, 1201−1218.

(16) Ragauskas, A. J.; Beckham, G. T.; Biddy, M. J.; Chandra, R.; Chen, F.; Davis, M. F.; Davison, B. H.; Dixon, R. A.; Gilna, P.; Keller, M.; Langan, P.; Naskar, A. K.; Saddler, J. N.; Tschaplinski, T. J.; Tuskan, G. A.; Wyman, C. E. Lignin Valorization: Improving Lignin Processing in the Biorefinery. *Science* **2014**, *344*, 1246843.

(17) Langholtz, M.; Downing, M.; Graham, R.; Baker, F.; Compere, A.; Griffith, W.; Boeman, R.; Keller, M. Lignin-Derived Carbon Fiber as a Co-Product of Refining Cellulosic Biomass. *SAE Int. J. Mater. Manf.* **2014**, *7*, 115−121.

(18) Gillet, S.; Aguedo, M.; Petitjean, L.; Morais, A. R. C.; da Costa Lopes, A. M.; Łukasik, R. M.; Anastas, P. T. Lignin transformations for high value applications: towards targeted modifications using green chemistry. *Green Chem.* **2017**, *19*, 4200−4233.

(19) Gadioli, R.; Waldman, W. R.; De Paoli, M. A. Lignin as a green primary antioxidant for polypropylene. *J. Appl. Polym. Sci.* **2016**, *133*, 43558.

(20) Liu, L.; Qian, M.; Song, P. a.; Huang, G.; Yu, Y.; Fu, S. Fabrication of Green Lignin-based Flame Retardants for Enhancing the Thermal and Fire Retardancy Properties of Polypropylene/Wood Composites. *ACS Sustainable Chem. Eng.* **2016**, *4*, 2422−2431.

(21) Yu, C.; Wang, F.; Zhang, C.; Fu, S.; Lucia, L. A. The synthesis and absorption dynamics of a lignin-based hydrogel for remediation of cationic dye-contaminated effluent. *React. Funct. Polym.* **2016**, *106*, 137−142.

(22) Domínguez-Robles, J.; Peresin, M. S.; Tamminen, T.; Rodríguez, A.; Larrañeta, E.; Jääskeläinen, A.-S. Lignin-based hydrogels with "super-swelling" capacities for dye removal. *Int. J. Biol. Macromol.* **2018**, *115*, 1249−1259.

(23) Andrady, A. L.; Pandey, K. K.; Heikkilä, A. M. Interactive effects of solar UV radiation and climate change on material damage. *Photochem. Photobiol. Sci.* **2019**, *18*, 804−825.

(24) Figueiredo, P.; Lintinen, K.; Hirvonen, J. T.; Kostiainen, M. A.; Santos, H. A. Properties and chemical modifications of lignin: Towards lignin-based nanomaterials for biomedical applications. *Prog. Mater. Sci.* **2018**, *93*, 233−269.

(25) Buono, P.; Duval, A.; Verge, P.; Averous, L.; Habibi, Y. New Insights on the Chemical Modification of Lignin: Acetylation versus Silylation. *ACS Sustainable Chem. Eng.* **2016**, *4*, 5212−5222.

(26) Liu, Z.; Zhao, L.; Cao, S.; Wang, S.; Li, P. Preparation and Evaluation of a Novel Cationic Amphiphilic Lignin Derivative with High Surface Activity. *BioResources* **2013**, *8*, 513.

(27) Ye, X.-X.; Luo, W.; Lin, L.; Zhang, Y.-q.; Liu, M.-h. Quaternized lignin-based dye dispersant: Characterization and performance research. *J. Dispersion Sci. Technol.* **2017**, *38*, 852−859.

(28) Ge, Y.; Song, Q.; Li, Z. A Mannich base biosorbent derived from alkaline lignin for lead removal from aqueous solution. *J. Ind. Eng. Chem.* **2015**, *23*, 228−234.

(29) Tao, X.; Shi, L. S.; Sun, M. J.; Li, N. Synthesis of Lignin Amine Asphalt Emulsifier and its Investigation by Online FTIR Spectrophotometry. *Adv. Mater. Res.* **2014**, *909*, 72−76.

(30) Liu, Z.; Lu, X.; An, L.; Xu, C. A Novel Cationic Lignin-amine Emulsifier with High Performance Reinforced via Phenolation and Mannich Reactions. *BioResources* **2016**, *11*, 6438.

(31) Seemala, B.; Meng, X.; Parikh, A.; Nagane, N.; Kumar, R.; Wyman, C. E.; Ragauskas, A.; Christopher, P.; Cai, C. M. Hybrid Catalytic Biorefining of Hardwood Biomass to Methylated Furans and Depolymerized Technical Lignin. *ACS Sustainable Chem. Eng.* **2018**, *6*, 10587−10594.

(32) Meng, X.; Parikh, A.; Seemala, B.; Kumar, R.; Pu, Y.; Wyman, C. E.; Cai, C. M.; Ragauskas, A. J. Characterization of fractional cuts of co-solvent enhanced lignocellulosic fractionation lignin isolated by sequential precipitation. *Bioresour. Technol.* **2019**, *272*, 202−208.

https://dx.doi.org/10.1021/acsomega.9b03717
ACS Omega 2020, 5, 2865−2877

(33) Ataeefard, M.; Shadman, A.; Saeb, M. R.; Mohammadi, Y. A hybrid mathematical model for controlling particle size, particle size distribution, and color properties of toner particles. *Appl. Phys. A* **2016**, *122*, 726.
(34) Hosseinnezhad, M.; Shadman, A.; Saeb, M. R.; Mohammadi, Y. A new direction in design and manufacture of co-sensitized dye solar cells: Toward concurrent optimization of power conversion efficiency and durability. *Opto-Electron. Rev.* **2017**, *25*, 229−237.
(35) Du, X.; Li, J.; Lindström, M. E. Modification of industrial softwood kraft lignin using Mannich reaction with and without phenolation pretreatment. *Ind. Crops Prod.* **2014**, *52*, 729−735.
(36) Zhou, W.; Chen, F.; Zhang, H.; Wang, J. Preparation of a Polyhydric Aminated Lignin and Its Use in the Preparation of Polyurethane Film. *J. Wood Chem. Technol.* **2017**, *37*, 323−333.
(37) Jiao, G.-J.; Peng, P.; Sun, S.-L.; Geng, Z.-C.; She, D. Amination of biorefinery technical lignin by Mannich reaction for preparing highly efficient nitrogen fertilizer. *Int. J. Biol. Macromol.* **2019**, *127*, 544−554.
(38) Qiao, X.; Zhao, C.; Shao, Q.; Hassan, M. Structural Characterization of Corn Stover Lignin after Hydrogen Peroxide Presoaking Prior to Ammonia Fiber Expansion Pretreatment. *Energy Fuels* **2018**, *32*, 6022−6030.
(39) Wang, X.; Zhang, Y.; Hao, C.; Dai, X.; Zhou, Z.; Si, N. Ultrasonic-assisted synthesis of aminated lignin by a Mannich reaction and its decolorizing properties for anionic azo-dyes. *RSC Adv.* **2014**, *4*, 28156−28164.
(40) Chatterjee, M.; Ishizaka, T.; Kawanami, H. Reductive amination of furfural to furfurylamine using aqueous ammonia solution and molecular hydrogen: an environmentally friendly approach. *Green Chem.* **2016**, *18*, 487−496.
(41) Constant, S.; Wienk, H. L. J.; Frissen, A. E.; Peinder, P. d.; Boelens, R.; van Es, D. S.; Grisel, R. J. H.; Weckhuysen, B. M.; Huijgen, W. J. J.; Gosselink, R. J. A.; Bruijnincx, P. C. A. New insights into the structure and composition of technical lignins: a comparative characterisation study. *Green Chem.* **2016**, *18*, 2651−2665.
(42) Meng, X.; Evans, B. R.; Yoo, C. G.; Pu, Y.; Davison, B. H.; Ragauskas, A. J. Effect of in Vivo Deuteration on Structure of Switchgrass Lignin. *ACS Sustainable Chem. Eng.* **2017**, *5*, 8004−8010.
(43) Yoo, C. G.; Li, M.; Meng, X.; Pu, Y.; Ragauskas, A. J. Effects of organosolv and ammonia pretreatments on lignin properties and its inhibition for enzymatic hydrolysis. *Green Chem.* **2017**, *19*, 2006−2016.
(44) Sun, S.; Huang, Y.; Sun, R.; Tu, M. The strong association of condensed phenolic moieties in isolated lignins with their inhibition of enzymatic hydrolysis. *Green Chem.* **2016**, *18*, 4276−4286.
(45) Wang, X.; Guo, Y.; Zhou, J.; Sun, G. Structural changes of poplar wood lignin after supercritical pretreatment using carbon dioxide and ethanol-water as co-solvents. *RSC Adv.* **2017**, *7*, 8314−8322.
(46) Wildschut, J.; Smit, A. T.; Reith, J. H.; Huijgen, W. J. J. Ethanol-based organosolv fractionation of wheat straw for the production of lignin and enzymatically digestible cellulose. *Bioresour. Technol.* **2013**, *135*, 58−66.
(47) Meng, X.; Parikh, A.; Seemala, B.; Kumar, R.; Pu, Y.; Christopher, P.; Wyman, C. E.; Cai, C. M.; Ragauskas, A. J. Chemical Transformations of Poplar Lignin during Cosolvent Enhanced Lignocellulosic Fractionation Process. *ACS Sustainable Chem. Eng.* **2018**, *6*, 8711−8718.
(48) Balakshin, M.; Capanema, E. On the Quantification of Lignin Hydroxyl Groups With 31P and 13C NMR Spectroscopy. *J. Wood Chem. Technol.* **2015**, *35*, 220−237.
(49) Bian, H.; Chen, L.; Gleisner, R.; Dai, H.; Zhu, J. Y. Producing wood-based nanomaterials by rapid fractionation of wood at 80 °C using a recyclable acid hydrotrope. *Green Chem.* **2017**, *19*, 3370−3379.
(50) Wang, Y.-Y.; Li, M.; Wyman, C. E.; Cai, C. M.; Ragauskas, A. J. Fast Fractionation of Technical Lignins by Organic Cosolvents. *ACS Sustainable Chem. Eng.* **2018**, *6*, 6064−6072.
(51) Cao, J.; Xiao, G.; Xu, X.; Shen, D.; Jin, B. Study on carbonization of lignin by TG-FTIR and high-temperature carbonization reactor. *Fuel Process. Technol.* **2013**, *106*, 41−47.
(52) Kajihara, M.; Aoki, D.; Matsushita, Y.; Fukushima, K. Synthesis and characterization of lignin-based cationic dye-flocculant. *J. Appl. Polym. Sci.* **2018**, *135*, 46611.
(53) Prola, L. D. T.; Machado, F. M.; Bergmann, C. P.; de Souza, F. E.; Gally, C. R.; Lima, E. C.; Adebayo, M. A.; Dias, S. L. P.; Calvete, T. Adsorption of Direct Blue 53 dye from aqueous solutions by multi-walled carbon nanotubes and activated carbon. *J. Environ. Manage.* **2013**, *130*, 166−175.
(54) Li, X.; He, Y.; Sui, H.; He, L. One-Step Fabrication of Dual Responsive Lignin Coated Fe_3O_4 Nanoparticles for Efficient Removal of Cationic and Anionic Dyes. *Nanomaterials* **2018**, *8*, 162.
(55) Olivo-Alanis, D.; Garcia-Reyes, R. B.; Alvarez, L. H.; Garcia-Gonzalez, A. Mechanism of anaerobic bio-reduction of azo dye assisted with lawsone-immobilized activated carbon. *J. Hazard. Mater.* **2018**, *347*, 423−430.
(56) Vahidhabanu, S.; Adeogun, A. I.; Babu, B. R. Biopolymer-Grafted, Magnetically Tuned Halloysite Nanotubes as Efficient and Recyclable Spongelike Adsorbents for Anionic Azo Dye Removal. *ACS Omega* **2019**, *4*, 2425−2436.
(57) Goscianska, J.; Pietrzak, R. Removal of tartrazine from aqueous solution by carbon nanotubes decorated with silver nanoparticles. *Catal. Today* **2015**, *249*, 259−264.
(58) Asfaram, A.; Ghaedi, M.; Dashtian, K.; Ghezelbash, G. R. Preparation and Characterization of Mn0.4Zn0.6Fe2O4 Nanoparticles Supported on Dead Cells of Yarrowia lipolytica as a Novel and Efficient Adsorbent/Biosorbent Composite for the Removal of Azo Food Dyes: Central Composite Design Optimization Study. *ACS Sustainable Chem. Eng.* **2018**, *6*, 4549−4563.
(59) Mahmoodi, N. M.; Roudaki, M. S. M. A.; Didehban, K.; Saeb, M. R. Ethylenediamine/glutaraldehyde-modified starch: A bioplatform for removal of anionic dyes from wastewater. *Korean J. Chem. Eng.* **2019**, *36*, 1421−1431.
(60) Dotto, G. L.; Vieira, M. L. G.; Pinto, L. A. A. Kinetics and Mechanism of Tartrazine Adsorption onto Chitin and Chitosan. *Ind. Eng. Chem. Res.* **2012**, *51*, 6862−6868.
(61) Oladipo, A. A.; Gazi, M.; Yilmaz, E. Single and binary adsorption of azo and anthraquinone dyes by chitosan-based hydrogel: Selectivity factor and Box-Behnken process design. *Chem. Eng. Res. Des.* **2015**, *104*, 264−279.
(62) Konicki, W.; Cendrowski, K.; Chen, X.; Mijowska, E. Application of hollow mesoporous carbon nanospheres as an high effective adsorbent for the fast removal of acid dyes from aqueous solutions. *Chem. Eng. J.* **2013**, *228*, 824−833.
(63) Zhao, J.; Lu, Z.; He, X.; Zhang, X.; Li, Q.; Xia, T.; Zhang, W.; Lu, C. Fabrication and Characterization of Highly Porous Fe(OH)3@ Cellulose Hybrid Fibers for Effective Removal of Congo Red from Contaminated Water. *ACS Sustainable Chem. Eng.* **2017**, *5*, 7723−7732.
(64) Wang, Y.; Zhu, L.; Wang, X.; Zheng, W.; Hao, C.; Jiang, C.; Wu, J. Synthesis of aminated calcium lignosulfonate and its adsorption properties for azo dyes. *J. Ind. Eng. Chem.* **2018**, *61*, 321−330.
(65) Wang, Z.; Hou, L.; Liu, Y.; Wang, Y.; Ma, L. Q.; Wu, J. Metal contamination in a riparian wetland: Distribution, fractionation and plant uptake. *Chemosphere* **2018**, *200*, 587−593.
(66) Meng, X.; Crestini, C.; Ben, H.; Hao, N.; Pu, Y.; Ragauskas, A. J.; Argyropoulos, D. S. Determination of hydroxyl groups in biorefinery resources via quantitative 31P NMR spectroscopy. *Nat. Protoc.* **2019**, *14*, 2627−2647.

https://dx.doi.org/10.1021/acsomega.9b03717
ACS Omega 2020, 5, 2865−2877